Many-Electron QED Corrections to the g Factor of Lithiumlike Ions

A. V. Volotka,[1,2] D. A. Glazov,[1,2,3] V. M. Shabaev,[2] I. I. Tupitsyn,[2] and G. Plunien[1]
[1]*Institut für Theoretische Physik, Technische Universität Dresden, Mommsenstraße 13, D-01062 Dresden, Germany*
[2]*Department of Physics, St. Petersburg State University, Oulianovskaya 1, Petrodvorets, 198504 St. Petersburg, Russia*
[3]*Institute for Theoretical and Experimental Physics, NRC Kurchatov Institute, B. Cheremushkinskaya 25, 117218 Moscow, Russia*
(Received 29 April 2014; published 26 June 2014)

A rigorous QED evaluation of the two-photon exchange corrections to the g factor of lithiumlike ions is presented. The screened self-energy corrections are calculated for the intermediate-Z region, and its accuracy for the high-Z region is essentially improved in comparison with that of previous calculations. As a result, the theoretical accuracy of the g factor of lithiumlike ions is significantly increased. The theoretical prediction obtained for the g factor of $^{28}Si^{11+}$ $g_{\rm th} = 2.000\,889\,892(8)$ is in an excellent agreement with the corresponding experimental value $g_{\rm exp} = 2.000\,889\,889\,9(21)$ [A. Wagner *et al.*, Phys. Rev. Lett. 110, 033003 (2013)].

DOI: 10.1103/PhysRevLett.112.253004 PACS numbers: 31.30.J-, 31.15.ac, 31.30.js

Highly charged ions provide not only a unique scenario for probing QED effects in the strongest electromagnetic fields but also give access to an accurate determination of fundamental physical constants and nuclear parameters. In recent years, amazing progress has been made in the experimental and theoretical investigations of the bound-electron g factor. High-precision measurements of the ground-state g factor of H-like carbon [1] and oxygen [2] and the related theoretical calculations provided determination of the electron mass. Recently, due to the substantial progress in the experimental accuracy of the g factor of H-like carbon and silicon, the mass of the electron is once again substantially refined [3]. So far, H- and Li-like silicon ions represent the heaviest ions, where the g factor has been accurately measured [4–6]. To date, these experiments provide the most stringent tests of the bound-state QED (BS QED) corrections in the presence of a magnetic field. Accurate measurements of the g factor in few-electron ions, such as Li-like calcium and B-like argon [7], are already anticipated. The investigations of the few-electron ions, unlike H-like ions, also provide access to the many-electron QED corrections, which are represented by a different facet of the QED diagrams.

The theoretical contributions to the g factor of Li-like ions can be separated into one-electron and many-electron parts. The one-electron terms are similar to the corresponding corrections to the g factor of H-like ions. The many-electron contributions, which define the main difference between the g factors of H- and Li-like ions, were investigated in Refs. [8–13]. The many-electron contributions are mainly determined by the screened radiative and the interelectronic-interaction corrections. For low-Z ions, the screened radiative corrections were obtained by employing the perturbation theory to the leading orders in αZ [9,10]. For intermediate-Z ions, the screening effect was evaluated by introducing the effective screening potential in the QED calculations to all orders in αZ [11]. For high-Z ions, the most accurate results for the screened radiative corrections were obtained rigorously within a systematic QED approach [12,13]. The one-photon exchange diagrams, which represent the interelectronic-interaction correction of the first order in $1/Z$, were evaluated in the framework of QED in Ref. [8]. The second- and higher-order contributions of the interelectronic interaction were calculated by means of the large-scale configuration-interaction Dirac-Fock-Sturm method in Ref. [10]. However, until now, for all values of Z, the theoretical uncertainty was determined by the interelectronic-interaction corrections and also, for the intermediate-Z region, by the screened self-energy corrections. In the present Letter, we report on the complete evaluation of the two-photon exchange and the screened self-energy corrections in the framework of a rigorous QED approach within an extended Furry picture.

In the extended Furry picture, to zeroth order, we solve the Dirac equation with an effective spherically symmetric potential, treating the interaction with the external Coulomb potential of the nucleus and the local screening potential as exact to all orders. This approach significantly accelerates the convergence of the perturbation expansion. We use different types of the screening potential. The simplest choice is the core-Hartree (CH) potential, which is created by the charge density distribution of the two core electrons in the $1s$ state. Other choices are the x_α potentials: Kohn-Sham, Dirac-Hartree, and Dirac-Slater, which were successfully employed in previous calculations of highly charged ions [11,14–19]. Moreover, we have also employed the Perdew-Zunger (PZ) potential [20] and the local Dirac-Fock (LDF) potential derived by inversion of the radial Dirac equation [21].

Let us now turn to the evaluation of the two-photon exchange corrections to the g factor of Li-like ions. These

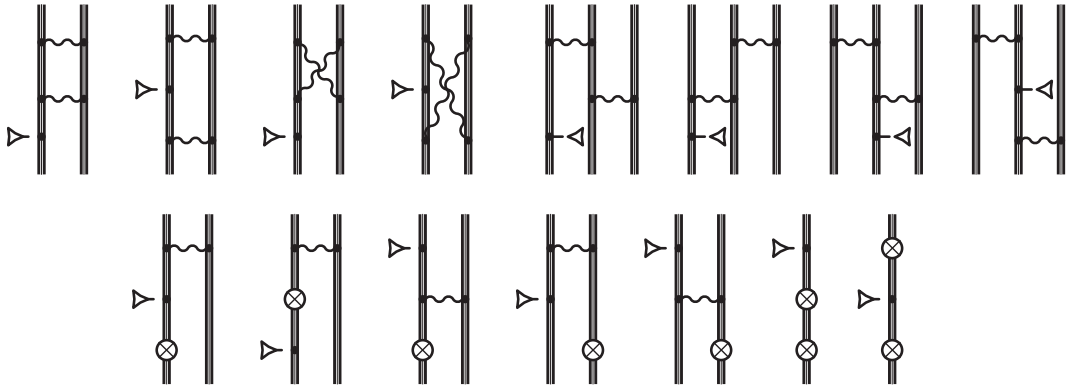

FIG. 1. Feynman diagrams representing the second-order interelectronic-interaction corrections to the g factor in local effective potentials. The wavy line indicates the photon propagator, and the triple lines describe the electron propagators in the effective potential. The dashed line terminated with the triangle denotes the interaction with the magnetic field. The counterterm diagrams are depicted in the second line. The symbol the circled cross represents the extra interaction term associated with the screening potential counterterm.

corrections are defined by diagrams of third order in the QED perturbation theory. The corresponding diagrams are presented in Fig. 1. The electron propagators in the figure have to be treated in the effective potential (we indicate this diagrammatically via the triple-electron line). In contrast to the case of the original Furry picture, in the extended Furry picture, the additional counterterm diagrams appear. These diagrams are depicted in the second line in Fig. 1. They are associated with an extra interaction term represented graphically by the symbol $\otimes$. Taking into account all possible permutations of the one-electron states, in total, we have to evaluate 36 three-electron, 36 two-electron, and 2 one-electron diagrams, respectively. All together, these diagrams form the complete gauge invariant set of the two-photon exchange contributions. The most difficult ones are the 16 two-electron diagrams depicted in the first line in Fig. 1. Each of these diagrams contains a threefold summation over the complete Dirac spectrum and an integration over the loop energy. Formal expressions for the diagrams in the first line are similar to those derived for the corresponding calculation of the hyperfine splitting and can be found in Ref. [22]. The formulas derived there can be taken over, but, instead of the hyperfine-interaction potential, we employ here the interaction with a constant magnetic field and keep in mind that the Dirac spectrum is now generated by solving the Dirac equation with the effective potential. The derivation of the formal expressions for the diagrams of the second line is straightforward and will be presented elsewhere. More details about the scheme of the numerical implementations can be found in Ref. [22]. However, unlike the hyperfine splitting, in the case of the g factor, the calculations are more involved due to the large cancellations of various terms and poor convergence of the partial-wave expansion. Nevertheless, we have substantially increased the accuracy of all the numerical integrations and extended the partial-wave summation up to $\kappa_{\max} = 15$. For a consistency check, we performed calculations both in Feynman and Coulomb gauges, and the results are found to be gauge invariant with a very high accuracy.

In Table I, the interelectronic-interaction corrections to the g factor of Li-like silicon are given. The results are obtained with four different starting potentials: Coulomb, core-Hartree, Perdew-Zunger, and local Dirac-Fock potentials. In the extended Furry picture, the interelectronic interaction contributes already in the zeroth order, due to the presence of the screening potential in the Dirac equation. The one-photon (first-order) and two-photon (second-order) exchange corrections have been evaluated to all orders in αZ in the framework of a rigorous QED approach. The higher-order corrections have been extracted from the calculations performed by means of the large-scale

TABLE I. Interelectronic-interaction corrections to the ground-state g factor of the Li-like $^{28}Si^{11+}$ ion in various starting potentials in units 10^{-6}.

	Coulomb	CH	PZ	LDF
Zeroth order		348.267	321.632	349.636
First order	321.592	−33.549	−5.990	−33.846
Second order	−6.876	0.137	−0.866	−0.976
Higher orders	0.085(22)	−0.046(6)	0.034(6)	−0.005(6)
Total	314.801(22)	314.809(6)	314.810(6)	314.808(6)

configuration-interaction Dirac-Fock-Sturm method described in Refs. [10,23]. As it was expected, the employment of the extended Furry picture increases the convergence of the perturbation expansion. This allows us to reduce the absolute uncertainty of the higher-order interelectronic-interaction corrections. Finally, the rigorous evaluation of the two-photon exchange corrections and the improved calculations of the higher-order terms allow us to significantly increase the total accuracy of the interelectronic-interaction terms for all ions under consideration. For example, in the case of the $^{28}Si^{11+}$ ion, the previous result was 0.000 314 903(74) [10], while the present calculation yields 0.000 314 809(6), and in the case of the $^{208}Pb^{79+}$ ion, instead of the previous value 0.002 140 7(27) [10], we now receive 0.002 139 34(4).

Let us now turn to the screened self-energy corrections to the g factor of Li-like ions. In Refs. [12,13], these corrections have been rigorously evaluated only for the $^{208}Pb^{79+}$ and $^{238}U^{89+}$ ions. The reasons for this are twofold. The first reason is the large numerical cancellations which occur in the point-by-point difference; the second is the poor convergence of the partial-wave expansion. In order to overcome these problems, we have performed the calculations in the extended Furry picture and employed a special treatment of the many-potential terms. The Feynman diagrams in the extended Furry picture corresponding to the screened self-energy corrections to the g factor are presented in Fig. 2. The corresponding expressions derived in Refs. [12,13] remain formally the same but keep in mind that the Dirac spectrum is now generated by solving the Dirac equation with the effective potential. In the second line of Fig. 2, the additional counterterm diagrams are depicted. The derivation of the formal expressions for them is relatively simple and will be presented elsewhere. The employment of the extended Furry picture allows us to substantially reduce the numerical cancellations of different terms as well as to improve convergence of the partial-wave expansion. However, in order to improve the convergence even further, we have employed a specific treatment of some many-potential terms. The standard way to treat the vertex and reducible corrections is to separate terms (zero-potential contributions) in which bound-electron propagators are replaced by free propagators. The remaining many-potential terms being ultraviolet finite are generally calculated directly in coordinate space [24]. However, for gaining better control over the partial-wave summation, we also separate the so-called one-potential contributions. In this way, the one-potential terms are treated in the momentum space. Such treatment of the one-potential term was applied in previous calculations of the one-electron self-energy corrections to the g factor in Refs. [25–29] and to the magnetic-dipole transition amplitude in Ref. [30]. Here, we extend this procedure to the evaluation of the screened self-energy corrections to the g factor. Performing the analysis of the convergence of the partial-wave expansion for different terms, we have found that such treatment should be applied to the terms $(C1)$ [Eq. (32)], $(H3)$ [Eq. (38)], $(I1)$ [Eq. (47)], and $(I3)$ [Eq. (49)] in Ref. [13]. The corresponding one-potential contributions of the self-energy (SE) part of the screened QED (SQED) corrections are given by the expressions

$$\begin{aligned}\Delta E^{\mathrm{SE}(C1)(1)}_{\mathrm{SQED}} = -8\pi i\alpha \sum_P (-1)^P \int \frac{d^3p\, d^3p'\, d^3q\, d^4k}{(2\pi)^{13}} \frac{1}{k^2} \\ \times \bar{\psi}_a(\mathbf{p})\gamma_\mu S_F(p-k)\gamma_0 [V_{\mathrm{eff}}(\mathbf{q}) S_F(p-k-q) \\ \times T_0(\mathbf{p}-\mathbf{p}'-\mathbf{q}) + T_0(\mathbf{q}) S_F(p-k-q) \\ \times V_{\mathrm{eff}}(\mathbf{p}-\mathbf{p}'-\mathbf{q})]\gamma_0 S_F(p'-k)\gamma^\mu \psi_{\zeta_{b|PaPb}}(\mathbf{p}') \\ + (a \leftrightarrow b), \end{aligned} \tag{1}$$

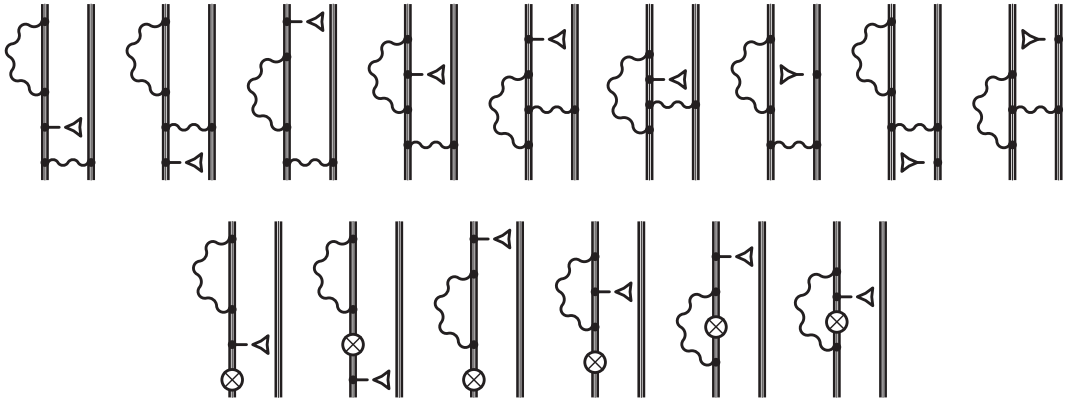

FIG. 2. Feynman diagrams representing the screened self-energy corrections to the g factor in local effective potentials. The wavy line indicates the photon propagator, and the triple lines describe the electron propagators in the effective potential. The dashed line terminated with the triangle denotes the interaction with the magnetic field. The counterterm diagrams are depicted in the second line. The symbol the circled cross represents the extra interaction term associated with the screening potential counterterm.

$$\Delta E^{\mathrm{SE}(H3)(1)}_{\mathrm{SQED}} = -8\pi i\alpha \int \frac{d^3p\,d^3p'\,d^4k}{(2\pi)^{10}} \frac{1}{k^2} \bar{\psi}_a(\mathbf{p}) \times \frac{\partial}{\partial\varepsilon_a}[\gamma_\mu S_F(p-k)\gamma_0 V_{\mathrm{eff}}(\mathbf{p}-\mathbf{p}')S_F(p'-k)\gamma^\mu] \times \psi_{\eta_a}(\mathbf{p}') + (a \leftrightarrow b), \quad (2)$$

$$\Delta E^{\mathrm{SE}(I1)(1)}_{\mathrm{SQED}} = -4\pi i\alpha \int \frac{d^3p\,d^3p'\,d^4k}{(2\pi)^{10}} \frac{1}{k^2} \bar{\psi}_a(\mathbf{p}) \frac{\partial}{\partial\varepsilon_a}[\gamma_\mu S_F(p-k) \times \gamma_0 T_0(\mathbf{p}-\mathbf{p}')S_F(p'-k)\gamma^\mu]\psi_a(\mathbf{p}') \times \sum_P (-1)^P \langle ab|I(\Delta)|PaPb\rangle + (a \leftrightarrow b), \quad (3)$$

$$\Delta E^{\mathrm{SE}(I3)(1)}_{\mathrm{SQED}} = -4\pi i\alpha \int \frac{d^3p\,d^4k}{(2\pi)^7} \frac{1}{k^2} \times \bar{\psi}_a(\mathbf{p}) \frac{\partial^2}{\partial\varepsilon_a^2}[\gamma_\mu S_F(p-k)\gamma^\mu]\psi_a(\mathbf{p}')\langle a|T_0|a\rangle \times \sum_P (-1)^P \langle ab|I(\Delta)|PaPb\rangle + (a \leftrightarrow b), \quad (4)$$

where $p = (\varepsilon_a, \mathbf{p})$, $p' = (\varepsilon_a, \mathbf{p}')$, $q = (\varepsilon_a, \mathbf{q})$, $\Delta = \varepsilon_a - \varepsilon_{Pa}$, and the notation $(a \leftrightarrow b)$ stands for the contribution with interchanged labels a and b; $\gamma^\mu = (\gamma_0, \boldsymbol{\gamma})$ are the Dirac matrices, $S_F(p) = (\gamma \cdot p - m)^{-1}$ is the free-electron propagator, the interelectronic-interaction operator $I(\varepsilon)$ and its derivatives are defined in a similar way as in Ref. [13], and V_{eff} is the effective potential, being the sum of the nuclear and screening potentials. T_0 is the operator of interaction with a constant magnetic field, which reads in the momentum space

$$T_0(\mathbf{p}) = i\mu_0(2\pi)^3[\boldsymbol{\alpha} \times \nabla_{\mathbf{p}}\delta^3(\mathbf{p})] \cdot \mathbf{H}, \quad (5)$$

where $\mu_0 = |e|/2$ is the Bohr magneton and $\mathbf{H}$ is the magnetic field directed along the z axis. The wave function $|\eta_a\rangle$ is given by the expression

$$|\eta_a\rangle = \sum_P (-1)^P \Big\{ |a\rangle \Big[\langle\zeta_{b|PaPb}|T_0|a\rangle + \langle\zeta_{a|PbPa}|T_0|b\rangle + \langle ab|I'(\Delta)|PaPb\rangle \Big(\langle a|T_0|a\rangle - \frac{1}{2}\langle b|T_0|b\rangle \Big) \Big] + |\xi_a\rangle\langle ab|I(\Delta)|PaPb\rangle + |\zeta_{b|PaPb}\rangle\langle a|T_0|a\rangle \Big\}, \quad (6)$$

and the wave functions $|\xi\rangle$ and $|\zeta\rangle$ are defined similarly to those in Ref. [12].

The ultraviolet-finite one-potential terms given by Eqs. (1)–(4) have been evaluated in the momentum space. The corresponding expressions in the coordinate space have been subtracted from the related many-potential terms by means of point-by-point difference. The partial-wave expansion for the many-potential terms was terminated at $\kappa_{\max} = 15$, and the remainder of the sum was estimated by a least-square polynomial fitting and by the ϵ algorithm of the Padé approximation. As a result, we have significantly increased the accuracy of the screened self-energy correction. In the case of the $^{28}Si^{11+}$ ion, the previous result was $-0.000\,000\,218(46)$ [10], while the present calculation yields $-0.000\,000\,242(5)$, and in the case of the $^{208}Pb^{79+}$ ion, instead of the previous value $-0.000\,003\,3(2)$ [12,13], we now receive $-0.000\,003\,44(2)$.

In Table II, the individual contributions and the total values of the g factor for Li-like silicon $^{28}Si^{11+}$, calcium $^{40}Ca^{17+}$, lead $^{208}Pb^{79+}$, and uranium $^{238}U^{89+}$ are presented together with the previously reported theoretical results and the experimental value for the case of silicon. The screened

TABLE II. Individual contributions to the ground-state g factor of Li-like ions and comparison with the previously reported theoretical values as well as with the experimental result for the $^{28}Si^{11+}$ ion.

	$^{28}Si^{11+}$	$^{40}Ca^{17+}$	$^{208}Pb^{79+}$	$^{238}U^{89+}$
Dirac value (point nucleus)	1.998 254 751	1.996 426 011	1.932 002 904	1.910 722 624
Finite nuclear size	0.000 000 003	0.000 000 014	0.000 078 57(14)	0.000 241 62(36)
QED, $\sim\alpha$	0.002 324 044	0.002 325 555(5)	0.002 411 7(1)	0.002 446 3(2)
QED, $\sim\alpha^2$	−0.000 003 517(1)	−0. 000 003 520(2)	−0.000 003 6(5)	−0.000 003 6(8)
Interelectronic interaction	0.000 314 809(6)	0.000 454 290(9)	0.002 139 34(4)	0.002 500 05(6)
Screened self-energy	−0.000 000 242(5)	−0.000 000 387(7)	−0.000 003 44(2)	−0.000 004 73(3)
Screened vacuum polarization	0.000 000 006	0.000 000 017	0.000 001 53(3)	0.000 002 55(5)
Nuclear recoil	0.000 000 039(1)	0.000 000 061(2)	0.000 000 25(35)	0.000 000 28(69)
Nuclear polarization			−0.000 000 04(2)	−0.000 000 27(14)
Total theory	2.000 889 892(8)	1.999 202 041(13)	1.936 627 2(6)	1.915 904 8(11)
	2.000 889 909(51)[a]	1.999 202 24(17)[b]	1.936 628 7(28)[c]	1.915 905 7(41)[c]
	2.000 890 005(87)[b]			
Experiment	2.000 889 889 9(21)[a]			

[a]Wagner *et al.* [6].
[b]Glazov *et al.* [10].
[c]Glazov *et al.* [13].

self-energy and interelectronic-interaction corrections calculated in this Letter allow us to substantially increase the theoretical accuracy for all ions under consideration. The other contributions to the g factor presented in Table II were considered in detail in our previous studies [10–13]. Comparison with the experimental value for a Li-like silicon ion provides tests of relativistic interelectronic interaction on a level of 10^{-5}, the one-electron BS QED on a level of 0.7%, and the screened BS QED on a level of 3%. Thus, the current studies provide the most accurate test of the many-electron QED effects in the case of the g factor. The further improvement of the g factor theory for Li-like ions requires at first the rigorous evaluation of the three-photon exchange diagrams and the subsequent betterment of the screened self-energy contribution for the intermediate-Z region, and the one-electron two-loop and nuclear recoil corrections for the high-Z region.

The techniques and numerical methods developed can also be extended for the g factor of B-like ions, where the corresponding studies can also lead to an independent determination of the fine-structure constant [31].

The work reported in this Letter was supported by DFG (Grant No. VO 1707/1-2), RFBR (Grants No. 13-02-00630 and No. 14-02-31316), and Saint Petersburg State University (Grants No. 11.0.15.2010 and No. 11.42.1225.2014). D. A. G. acknowledges financial support by the FAIR—Russia Research Center and by the "Dynasty" Foundation.

[1] H. Häffner, T. Beier, N. Hermanspahn, H.-J. Kluge, W. Quint, S. Stahl, J. Verdú, and G. Werth, Phys. Rev. Lett. **85**, 5308 (2000).
[2] J. Verdú, S. Djekić, S. Stahl, T. Valenzuela, M. Vogel, G. Werth, T. Beier, H.-J. Kluge, and W. Quint, Phys. Rev. Lett. **92**, 093002 (2004).
[3] S. Sturm, F. Köhler, J. Zatorski, A. Wagner, Z. Harman, G. Werth, W. Quint, C. H. Keitel, and K. Blaum, Nature (London) **506**, 467 (2014).
[4] S. Sturm, A. Wagner, B. Schabinger, J. Zatorski, Z. Harman, W. Quint, G. Werth, C. H. Keitel, and K. Blaum, Phys. Rev. Lett. **107**, 023002 (2011).
[5] S. Sturm, A. Wagner, M. Kretzschmar, W. Quint, G. Werth, and K. Blaum, Phys. Rev. A **87**, 030501(R) (2013).
[6] A. Wagner, S. Sturm, F. Köhler, D. A. Glazov, A. V. Volotka, G. Plunien, W. Quint, G. Werth, V. M. Shabaev, and K. Blaum, Phys. Rev. Lett. **110**, 033003 (2013).
[7] D. von Lindenfels, M. Wiesel, D. A. Glazov, A. V. Volotka, M. M. Sokolov, V. M. Shabaev, G. Plunien, W. Quint, G. Birkl, A. Martin, and M. Vogel, Phys. Rev. A **87**, 023412 (2013).
[8] V. M. Shabaev, D. A. Glazov, M. B. Shabaeva, V. A. Yerokhin, G. Plunien, and G. Soff, Phys. Rev. A **65**, 062104 (2002).
[9] Z.-C. Yan, J. Phys. B **35**, 1885 (2002).
[10] D. A. Glazov, V. M. Shabaev, I. I. Tupitsyn, A. V. Volotka, V. A. Yerokhin, G. Plunien, and G. Soff, Phys. Rev. A **70**, 062104 (2004).
[11] D. A. Glazov, A. V. Volotka, V. M. Shabaev, I. I. Tupitsyn, and G. Plunien, Phys. Lett. A **357**, 330 (2006).
[12] A. V. Volotka, D. A. Glazov, V. M. Shabaev, I. I. Tupitsyn, and G. Plunien, Phys. Rev. Lett. **103**, 033005 (2009).
[13] D. A. Glazov, A. V. Volotka, V. M. Shabaev, I. I. Tupitsyn, and G. Plunien, Phys. Rev. A **81**, 062112 (2010).
[14] J. Sapirstein and K. T. Cheng, Phys. Rev. A **63**, 032506 (2001).
[15] J. Sapirstein and K. T. Cheng, Phys. Rev. A **64**, 022502 (2001).
[16] J. Sapirstein and K. T. Cheng, Phys. Rev. A **66**, 042501 (2002).
[17] A. V. Volotka, D. A. Glazov, I. I. Tupitsyn, N. S. Oreshkina, G. Plunien, and V. M. Shabaev, Phys. Rev. A **78**, 062507 (2008).
[18] Y. S. Kozhedub, A. V. Volotka, A. N. Artemyev, D. A. Glazov, G. Plunien, V. M. Shabaev, I. I. Tupitsyn, and T. Stöhlker, Phys. Rev. A **81**, 042513 (2010).
[19] J. Sapirstein and K. T. Cheng, Phys. Rev. A **83**, 012504 (2011).
[20] J. P. Perdew and A. Zunger, Phys. Rev. B **23**, 5048 (1981).
[21] V. M. Shabaev, I. I. Tupitsyn, K. Pachucki, G. Plunien, and V. A. Yerokhin, Phys. Rev. A **72**, 062105 (2005).
[22] A. V. Volotka, D. A. Glazov, O. V. Andreev, V. M. Shabaev, I. I. Tupitsyn, and G. Plunien, Phys. Rev. Lett. **108**, 073001 (2012).
[23] I. I. Tupitsyn, A. V. Volotka, D. A. Glazov, V. M. Shabaev, G. Plunien, J. R. Crespo López-Urrutia, A. Lapierre, and J. Ullrich, Phys. Rev. A **72**, 062503 (2005).
[24] S. A. Blundell, K. T. Cheng, and J. Sapirstein, Phys. Rev. A **55**, 1857 (1997).
[25] H. Persson, S. Salomonson, P. Sunnergren, and I. Lindgren, Phys. Rev. A **56**, R2499 (1997).
[26] T. Beier, I. Lindgren, H. Persson, S. Salomonson, P. Sunnergren, H. Häffner, and N. Hermanspahn, Phys. Rev. A **62**, 032510 (2000).
[27] V. A. Yerokhin, P. Indelicato, and V. M. Shabaev, Phys. Rev. Lett. **89**, 143001 (2002).
[28] V. A. Yerokhin, P. Indelicato, and V. M. Shabaev, Phys. Rev. A **69**, 052503 (2004).
[29] V. A. Yerokhin and U. D. Jentschura, Phys. Rev. A **81**, 012502 (2010).
[30] A. V. Volotka, D. A. Glazov, G. Plunien, V. M. Shabaev, and I. I. Tupitsyn, Eur. Phys. J. D **38**, 293 (2006).
[31] V. M. Shabaev, D. A. Glazov, N. S. Oreshkina, A. V. Volotka, G. Plunien, H.-J. Kluge, and W. Quint, Phys. Rev. Lett. **96**, 253002 (2006).